Half-lives of ^{73}Sr and ^{76}Y and the consequences for the proton dripline

L. Sinclair,[1,2] R. Wadsworth,[1,*] J. Dobaczewski,[1,3,4] A. Pastore,[1] G. Lorusso,[2,5,6] H. Suzuki,[2] D. S. Ahn,[2] H. Baba,[2] F. Browne,[2,7] P. J. Davies,[1,†] P. Doornenbal,[2] A. Estrade,[8,‡] Y. Fang,[9,§] N. Fukuda,[2] J. Henderson,[1,‖] T. Isobe,[2] D. G. Jenkins,[1] S. Kubono,[2] Z. Li,[10] D. Lubos,[2,11] S. Nishimura,[2] I. Nishizuka,[12,¶] Z. Patel,[2,6] S. Rice,[2,6] H. Sakurai,[2] Y. Shimizu,[2] P. Schury,[2,#] H. Takeda,[2] P.-A. Söderström,[2,**] T. Sumikama,[13] H. Watanabe,[14] V. Werner,[15] J. Wu,[2,10] and Z. Y. Xu[16]

[1]*Department of Physics, University of York, Heslington, York, YO10 5DD, United Kingdom*
[2]*RIKEN Nishina Center, 2-1 Hirosawa, Wako, Saitama 351-0198, Japan*
[3]*Institute of Theoretical Physics, Faculty of Physics, University of Warsaw, ul. Pasteura 5, PL-02-093 Warsaw, Poland*
[4]*Helsinki Institute of Physics, P.O. Box 64, FI-00014 University of Helsinki, Finland*
[5]*National Physical Laboratory, Teddington, Middlesex TW11 0LW, United Kingdom*
[6]*Department of Physics, University of Surrey, Faculty of Engineering and Physical Sciences, Guildford GU2 7XH, United Kingdom*
[7]*School of Computing, Engineering and Mathematics, University of Brighton, Brighton BN2 4GJ, United Kingdom*
[8]*School of Physics and Astronomy, University of Edinburgh, Edinburgh EH8 9YL, United Kingdom*
[9]*Department of Physics, Osaka University, 1-1 Suita, Osaka Prefecture 565-0871, Japan*
[10]*School of Physics, Peking University, Physics Building, Peking University, Beijing 100871, China*
[11]*Technische Universität München, Boltzmannstr. 15, 85748 München, Germany*
[12]*Department of Physics, Tohoku University, 1-1-2-chome, Katahira, Aoba-ku, Sendai 980-0077, Japan*
[13]*Department of Physics, Tohoku University, 1-1-2-chome, Katahira, Aoba-ku, Sendai 980-0077, Japan*
[14]*Department of Physics, Beihang University, Beijing 100191, China*
[15]*Department of Physics, Yale University, New Haven, Connecticut 06511, USA*
[16]*University of Tokyo, 7-3-1 Hongo, Bunkyo, Tokyo 113-0033, Japan*

(Received 2 July 2019; published 16 October 2019)

The half-lives of seven nuclei have been determined in the neutron-deficient mass-70 region following their production via fragmentation of a 345 MeV/nucleon ^{124}Xe primary beam on a 740 mg/cm^2 ^{9}Be target at the RI Beam Factory, RIKEN. The results include two new (^{73}Sr and ^{76}Y) half-lives and a more precise measurement for the ground-state half-life of ^{74}Sr. The new results are discussed with reference to previously published calculations that predict the location of the proton dripline in the light Sr and Y region of the nuclear chart. In addition, differences in the ground-state structure of ^{72}Rb and ^{76}Y are discussed with the aid of density functional theory calculations. These provide a possible explanation for why ^{72}Rb undergoes proton decay while the α-conjugate nucleus ^{76}Y predominantly undergoes β^+ decay.

DOI: 10.1103/PhysRevC.100.044311

I. INTRODUCTION

Defining the boundaries of the limits of existence of atomic nuclei is one of the fundamental goals of low-energy nuclear physics research. On the proton-rich side of the so-called line of stability of the Segré chart of nuclides, knowledge of such boundaries is important, along with information on nuclear masses, lifetimes, and structure, for the understanding of the rapid-proton (rp) capture pathways that power type I x-ray bursts [1] occurring on the surface of accreting neutron stars. Under certain conditions, the rp-process path can extend up to about mass 100, generating x-ray bursts that can last several minutes [2].

In the present work the half-lives of ^{73}Sr and ^{76}Y, which reside close to the proton dripline, have been measured for the first time. In addition, a more precise ground-state half-life has been determined for the isotope ^{74}Sr along with further measurements for four other nuclei (^{70}Br, ^{71}Kr, ^{74}Rb, ^{75}Sr) [3–6], all of which are in agreement with the previously published values. The relatively long lifetime obtained in the

*rw10@york.ac.uk
†Present address: Department of Physics and Astronomy, University of Manchester, Manchester M13 9PL, United Kingdom.
‡Present address: Department of Physics, Central Michigan University, Mount Pleasant, MI 48859, USA.
§Present address: Department of Physics and Astronomy, State University of New York at Stony Brook, NY, USA.
‖Present address: Lawrence Livermore National Laboratory, 7000 East Ave, Livermore, CA 94550, USA.
¶Present address: GSI Helmholtzzentrum für Schwerionenforschung GmbH, 64291 Darmstadt, Germany.
#Present address: Institute of particle and Nuclear Studies (IPNS), High Energy Accelerator Research Organization (KEK), Ibaraki 305-0801, Japan.
**Present address: Extreme Light Infrastructure - Nuclear Physics (ELI-NP), 077125, Bucharest-Magurele, Romania.

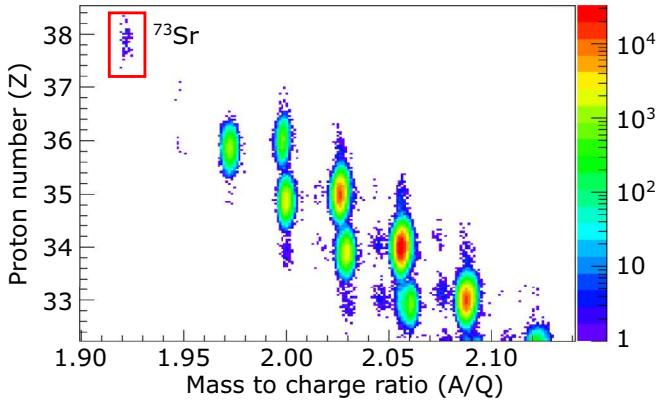

FIG. 1. BigRIPS particle identification spectrum obtained using the ^{73}Sr setting. The ions are identified with respect to proton number Z and mass-to-charge ratio A/Q. Nuclei with $A/Q = 2$ correspond to $N = Z$ nuclei. The nucleus ^{73}Sr is highlighted by the red box.

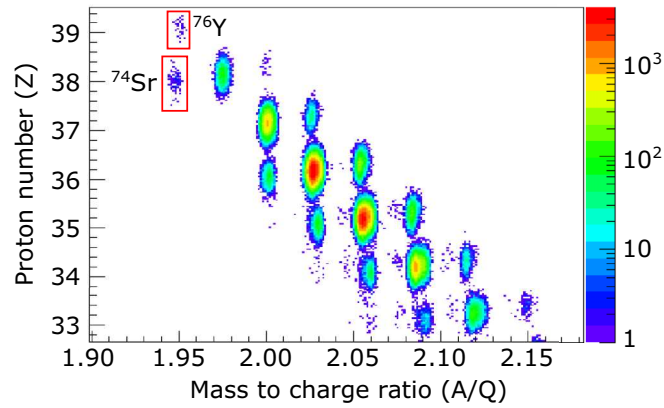

FIG. 2. Same as Fig. 1, but for the ^{74}Sr setting. The events associated with ^{74}Sr and ^{76}Y are highlighted by the red boxes.

present work for ^{76}Y is interesting in light of recent work published on the existence ^{72}Rb, which differs from ^{76}Y by only an α particle and has a lifetime of the order of 100 ns [7].

The data for the most exotic nuclei produced (^{73}Sr and ^{76}Y) are discussed with reference to theoretical predictions of the proton dripline in this region of the Segré chart. The experimentally observed difference in the half-lives and decay modes of the two nuclei ^{72}Rb and ^{76}Y are also discussed in terms of possible nuclear structure and deformation differences of the decaying states. This aspect is investigated with the aid of density functional theory (DFT) calculations under the assumption that it is the ground state in each nucleus that is involved in the decay process.

II. EXPERIMENT AND DATA ANALYSIS

The present results were obtained from an experiment performed at the radioactive-isotope beam factory (RIBF) at RIKEN. A primary ^{124}Xe beam with an energy of 345 MeV/u and intensity 30–35 pnA bombarded a 740 mg/cm^2 Be target to produce secondary beams via fragmentation. The fragments were separated according to their momenta and mass-to-charge ratio (A/Q) by the first stage of the in-flight RI projectile fragment separator (BigRIPS). The energy loss (ΔE), magnetic rigidity ($B\rho$), and time of flight (TOF) were measured using the second stage of BigRIPS and the zero-degree spectrometer (ZDS) giving the atomic number (Z) and A/Q of the individual ions by the ΔE-$B\rho$-TOF method [8]. The resultant particle identification (PID) plots are presented in Figs. 1 and 2 for the two transmission settings used, which were centered on ^{73}Sr and ^{74}Sr, respectively.

The experimental arrangement employed a β-counting system, the wide-range active silicon-strip stopper array for β and ion detection [9] (WAS3ABi) in conjunction with the γ-ray detection array EURICA (not used in the present work) at the ZDS focal plane to detect decay radiation from the individual ions. The heavy ions from the secondary beam were implanted into WAS3ABi which detected their subsequent β decay. WAS3ABi consisted of a double-sided silicon-strip detector (DSSSD), which had an active area of 62 × 62 mm^2, 16384 pixels, with a strip pitch of 485 μm and thickness of 1.0 mm.

To detect β decays below 100 keV [10] charge-sensitive preamplifiers (Clear-Pulse CS-520) and shaping amplifiers (CAEN N568B) were used [11]. To obtain β-decay trigger and timing information, inverted signals of the shaping amplifiers with a shaping time of 0.2 μs were fed into computer-automated measurement and control (CAMAC) leading-edge discriminators (LeCroy 3412, 4413) [12].

β-decay events were associated with preceding heavy-ion implantations based on position and time information from the active stopper, WAS3ABi. A prerequisite for the correlation analysis was the proper identification of the implanted ion species as shown in Figs. 1 and 2. The position correlation area consisted of the detector pixel where the implantation and decay event occurred, plus the four nearest neighbor pixels (two horizontal and two vertical). Given the low maximum implantation rate per pixel of about 4.3×10^{-3} Hz and the predicted β-decay rate the probability of multiple implantation events being correlated with a decay was negligible.

By correlating a sufficient number of implanted ions with the subsequent β decays, the data can be fit and a half-life can be extracted. In the current work all β decays observed within 1 s of an implanted ion were correlated. The time window of 1 s is chosen to include the parent, daughter, and, if appropriate, grand-daughter decays. Any other correlations found in this time window will form a time-random background. With a suitably low number the distribution of these time-random events will be uniform. Contaminants, produced by secondary reactions in the degrader, were expected to be implanted in the Si detector. An exponential background would be suitable if the radioactivity from the contaminants are not negligible; however, a constant background was found to be satisfactory in the present work. A similar method has been used previously; see, for example, [13]. Two fitting procedures can then be employed to extract the half-life. In the case of a large number of implanted ions and good correlations, a χ^2 fit of the exponential decay [14] is performed with daughter, granddaughter (if appropriate), and uniform background. For nuclei with very low yields, the half-lives were determined

TABLE I. Comparison of β-decay half-lives obtained in the present work $T_{1/2}^{\text{expt}}$ with the literature values $T_{1/2}^{\text{lit}}$. Values denoted by * are either calculated half-lives or limits placed on nuclei from previous experiments.

Nucleus	$T_{1/2}^{\text{lit}}$ (ms)	$T_{1/2}^{\text{expt}}$ (ms)	Method
^{70}Br	79.1(8) [3]	79.7(24)	χ^2
^{71}Kr	100(3) [4]	98.8(3)	χ^2
^{73}Sr	25* [21]	24.3(53)	χ^2
^{73}Sr	25* [21]	28^{+5}_{-4}	Schmidt
^{74}Sr	27(8) [17]	27.7(28)	χ^2
^{75}Sr	88(3) [6]	81.7(34)	χ^2
^{74}Rb	64.761(31) [5]	65.5(8)	χ^2
^{74}Rb	64.761(31) [5]	65.0(5)	Schmidt
^{76}Y	>200 ns* [20]	24^{+12}_{-6}	Schmidt

by the logarithmic binning method as described by Schmidt [15,16]. In this case the number of radioactive decay events is plotted against the natural logarithm of the time difference between ion implantation and β-particle detection. The mean lifetime (and hence the half-life) is then extracted from the centroid of the event distribution.

III. EXPERIMENTAL RESULTS

To test the suitability of the correlation and fitting procedures the ground-state decays of known nuclei were measured. For one of these nuclei (^{74}Rb) both the Schmidt and χ^2 methods were employed in order to compare results from the two methods. The half-lives $T_{1/2}$ obtained in the present work for ^{70}Br, ^{71}Kr, ^{74}Rb, and ^{75}Sr are summarized in Table I and an example of the data fitted using one of the methods discussed above for ^{70}Br is presented in Fig. 3. All of the measured half-lives in the present work are found to be in good agreement with the previously published literature values.

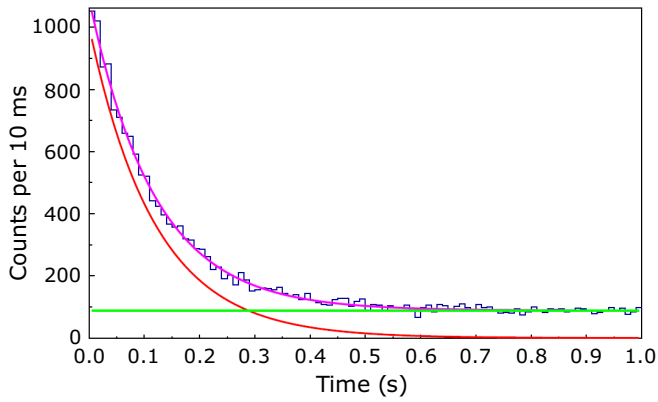

FIG. 3. Time distribution of the β-decay events following the identification of ^{70}Br nuclei in BigRIPS. Lower solid exponential curve (red line) - parent nuclei (data for the daughter nucleus is not included in the fit as the lifetime of ^{70}Se is 41 min), horizontal solid (green) line - constant back-ground. Upper most solid exponential curve (magenta line) - combined fit yielding $T_{1/2} = 79.7(24)$ ms for ^{70}Br.

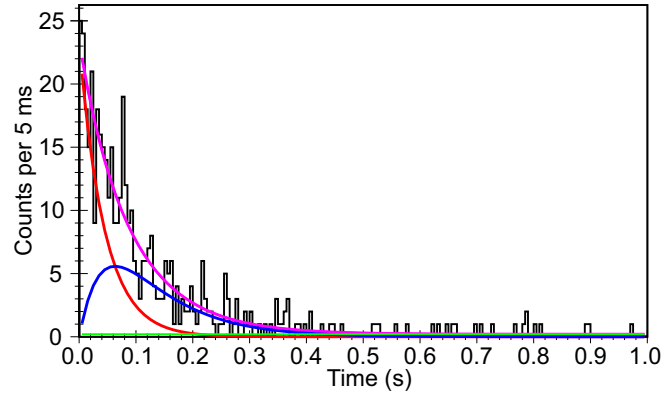

FIG. 4. Time distribution of the β-decay events following the identification of ^{74}Sr nuclei in BigRIPS. Lower solid exponetial curve (red line) - parent nuclei, ^{74}Sr. Exponentially rising/ faliing solid (blue) curve - daughter nuclei, ^{74}Rb with a known β-decay of 64.761(31) ms [5]; horizontal (green) line - constant background. Upper most solid exponential curve (magenta line) - combined fit yielding $T_{1/2} = 27.7(28)$ ms for ^{74}Sr.

The β^+-decay half-lives of nuclei ^{73}Sr and ^{76}Y have been measured for the first time. In addition, the ground-state lifetime of ^{74}Sr has been determined with higher precision than previous work [17].

Figure 4 shows the distribution of the β-decay events as a function of time following the implantation of ^{74}Sr nuclei. The β-decay fit of ^{74}Sr includes the activity of the daughter nuclide ^{74}Rb, whose β-decay half-life is known to be 64.761(31) ms [5]. A value of 27.7(28) ms is obtained for the half-life from the events observed in WAS3ABi that were correlated with β decays. In 2013 a previous in-beam study of ^{74}Sr was performed at Jyväskylä using the recoil-β-tagging technique. From the analysis of the γ rays, emitted at the target position, that were correlated with fast decays at the focal plane, and tentatively identified as being transitions in ^{74}Sr, an estimate of the lifetime was made. This resulted in a value of 27(8) ms [17] using the Schmidt method [15,16]. In the present work there is unambiguous identification of the events associated with the decay of ^{74}Sr. Knowledge of the half-life of ^{74}Sr is important for understanding the role of $2p$ capture on the rp-process waiting-point nucleus ^{72}Kr as discussed in [18]. In the latter work the impact of the half-life of ^{74}Sr on the effective half-life of ^{72}Kr was estimated to be about 10%.

In the present work the half-life of ^{73}Sr was obtained using both the χ^2 and Schmidt methods outlined in the previous section. Table I shows that consistent values, within errors, are obtained. Due to the low number of correlated events the half-life of ^{76}Y was determined using the Schmidt method [15,16], since this method is particularly useful for cases where there are limited statistics available. In this case, the number of radioactive decay events is plotted against the natural logarithm of the time differences between the implant and decay. The mean-lifetime (which can be converted to a half-life) is then extracted from the centroid of the event distribution. This method is useful when the parent and daughter have somewhat different half-lives. Data for ^{73}Sr and ^{76}Y analyzed via this method are presented in Fig. 5. A half-life of 28^{+5}_{-4} ms was

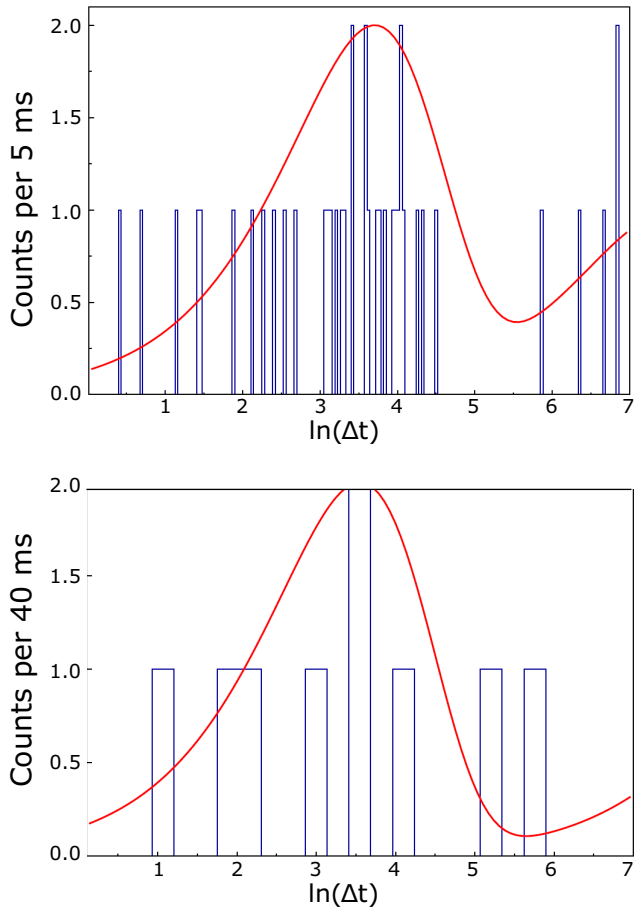

FIG. 5. Natural logarithm, $\ln(\Delta t)$, showing the time distribution of the correlated β-decay WASA3Bi events following the identification of ^{73}Sr nuclei (top) and ^{76}Y (bottom) events in BigRIPS. Δt is the time difference in ms between detection of the recoils and the β^+ events. The solid red curves show the best fit using the Schmidt method to extract the mean lifetimes. These were converted to half-life values of 28^{+5}_{-4} ms for ^{73}Sr (top) and 24^{+12}_{-6} ms for ^{76}Y (bottom), respectively. Note: The red curves have been multiplied by a factor to make them visible (the areas under the curve and in the data are not the same).

determined for ^{73}Sr from 42 β-decay WAS3ABi correlated events. In this case the daughter component was taken as ^{72}Kr with a $T_{1/2} = 17.1 \pm 0.2$ s [19] since ^{73}Rb is proton unbound (see Fig. 2). A $T_{1/2} = 24^{+12}_{-6}$ ms was extracted for ^{76}Y from a total of 9 β-decay WAS3ABi correlated events. For the latter nucleus the daughter component ($T_{1/2} = 7.9$ s) was included in the fitting procedure. [Note, the first identification of ^{76}Y was in [20] where two events were observed using the fragment recoil separator (FRS) following the fragmentation of a ^{112}Sn beam at GSI.]

IV. DISCUSSION

A. Proton dripline

The neutron-deficient isotopes under discussion reside in a region where, according to the finite-range droplet model (FRDM) plus folded Yukawa potential calculations, sizable ($\beta_2 \approx 0.40$) ground-state deformations are expected to exist [22]. These calculations also list the masses and binding energies of nuclei which can in turn be used to deduce the one- and two-proton separation energies. The latter values for ^{76,77}Y are all negative, suggesting that these nuclei are proton unbound, while for ^{73,74}Sr, positive one- and two-proton separation energies are predicted. Moving to lower masses ^{72}Sr is predicted to be bound by ≈0.8 MeV against one-proton emission but unbound against two-proton emission ($S_p \approx -0.7$ MeV). For even lighter Sr isotopes, ^{71}Sr is predicted to be unbound against both one- and two-proton decay.

Theoretical one- and two-proton separation energies have also been predicted in the mass-70 region using both Skyrme Hartree-Fock calculations [23] and more recently shell-model calculations using both the GXPF1A and JUN45 interactions [24]. In the former case ^{73,74}Sr are predicted to be bound against both one- and two-proton emission, while in the latter case ^{73}Sr is predicted to be unbound against two-proton decay. The HF calculations make no predictions for the Y isotopes, but the shell-model calculations (using the JUN45 interaction; see Fig. 3 from [24]) predict that ^{76,77}Y are unbound for one-proton emission. Interestingly relativistic Hartree-Bogoliubov calculations used to predict the proton dripline between $Z = 31$ and $Z = 49$ [25] suggest that ^{77}Y is proton bound and that the separation energy for ^{76}Y is almost zero (−0.03 MeV) and hence is on the border of being proton bound. Finally, the latest atomic mass table evaluation [26] extrapolates the one- and two-proton separation energies for ^{73,74}Sr as being positive but indicate that ^{76}Y has a negative one-proton separation energy. This latter conclusion remains true when the uncertainties quoted in the S_p values are taken into account.

Clearly the above results are not in total agreement regarding the location of the boundaries of existence of the light Sr and Y isotopes. However, the present lifetime measurements indicate that ^{73,74}Sr and ^{76}Y do not undergo proton decay, but prefer β^+ decay. The results for ^{73,74}Sr are in agreement with all of the above predictions [22–24,26]. On the other hand none of the models or mass evaluations predict that ^{76}Y is stable against one-proton decay and indeed several predict that ^{77}Y is also one-proton unbound, which is clearly not the case [27].

B. Decay properties of ^{72}Rb and ^{76}Y

The fact that ^{76}Y predominantly undergoes β decay with a ms lifetime while ^{72}Rb has a very short ≈100 ns lifetime [7] and presumably proton decays is very interesting. This difference in behavior most likely results from nuclear structure and/or deformation differences between the two isotopes, which differ from each other by an α particle. In the case of ^{72}Rb it was suggested that the state that undergoes proton decay could be a 5^+ state based on a dominant $\pi f_{\frac{5}{2}} \otimes \nu f_{\frac{5}{2}}$ configuration; however, a 9^+ state with dominant $\pi g_{\frac{9}{2}} \otimes \nu g_{\frac{9}{2}}$ configuration [7] could not be totally ruled out but was deemed to be a less likely explanation. For ^{77}Y, calculations presented in [28] suggest that the β-decaying ground state is predominantly based on the deformed Nilsson

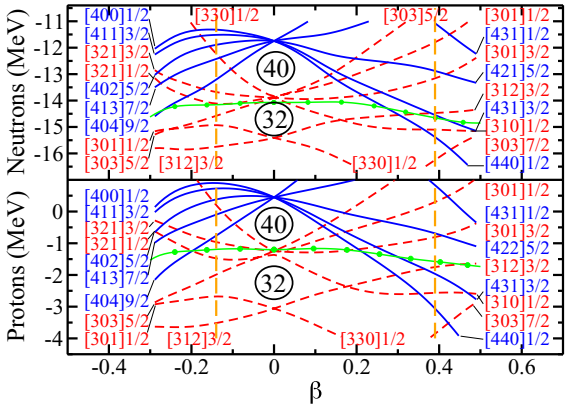

FIG. 6. Neutron (upper panel) and proton (lower panel) single-particle levels as functions of deformation β calculated for ^{72}Rb using Skyrme functional UNEDF0 [30]. The positive (negative) parity levels are marked by solid (dashed) lines and dominating Nilsson labels, see text. The dots indicate the Fermi energies. The dashed vertical lines indicate the positions of the lower and higher deformation energy minima shown in Fig. 8.

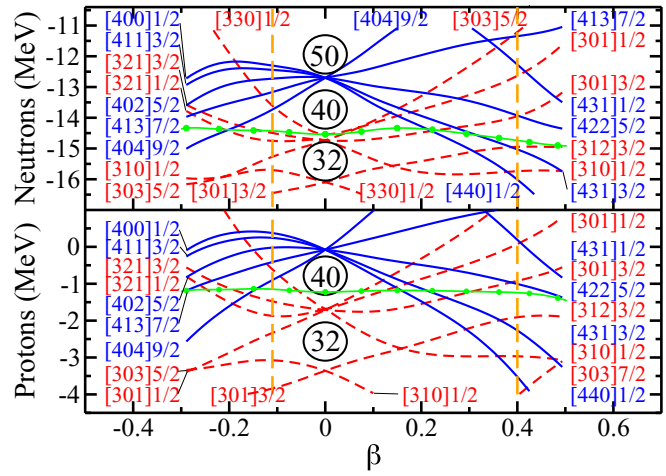

FIG. 7. Same as in Fig 6, but for ^{76}Y.

$[422]\frac{5}{2}^+$ orbital, which originates from the spherical $g_{\frac{9}{2}}$ orbit. Furthermore, we note that on approaching the higher mass (and more deformed) midshell region just below $A = 80$ it is highly likely that the changing Fermi surface (and deformation) could increase the importance of the $g_{\frac{9}{2}}$ orbit component contributions to the wave functions of the states in ^{76}Y. This in turn might explain the change in half-lives observed between the two isotopes (i.e., due to the higher angular momentum barrier) even if both involve decay from an excited 5^+ state. Finally, it is interesting to note that ^{78}Y possesses a low-lying 5^+ state that is isomeric and undergoes β^+ decay [29].

1. New theoretical approach

Unfortunately calculations of decay energies available in the literature do not allow us to obtain a consistent and reliable picture that would be fully compatible with experimental data. One should remember that the balance between proton emission and β decay is extremely sensitive to the decay energies, and thus the high theoretical precision required is probably beyond the capabilities of the current modeling techniques. Therefore, below we concentrate on other theoretical results, which can be more robust than those available for decay energies. However, before discussing the details of the calculations it is important to note that what follows is based on an assumption that it is the ground states that are involved in the decay processes.

In Figs. 6 and 7, we present Nilsson diagrams calculated for the Skyrme functional UNEDF0 [30] in ^{72}Rb and ^{76}Y, respectively. Calculations were performed in the so-called false-vacuum approximation, whereby the quasiparticle levels were not blocked, whereas when pairing is introduced the HFB + LN average proton and neutron numbers were set to be equal to those of the studied odd-odd nuclei. On the prolate side, the calculations clearly show three positive-parity down-sloping intruder Nilsson levels [440]1/2, [431]3/2, and [422]5/2, which originate from the spherical $g_{\frac{9}{2}}$ orbital. These states are crossed by several negative-parity up-sloping Nilsson levels originating from the fp spherical shell. Similarly, on the oblate side, the positive-parity levels [402]5/2, [404]7/2, and [404]9/2 are crossed by negative-parity levels [321]1/2 and [321]3/2.

To study a possible range of variations between different models, we performed analogous calculations for several different Skyrme functionals and for the phenomenological Woods-Saxon mean field. The obtained exact crossing points depend on very detailed properties of relative positions and deformation dependences of the Nilsson levels. Nevertheless, the overall general picture appears to be the same as that obtained for UNEDF0.

In Fig. 8, we show the calculated deformation energies in ^{72}Rb and ^{76}Y. The obtained values are fairly flat: i.e., between $\beta \approx -0.3$ and 0.5 all deformation energies are between -1 and $+1$ MeV. Nevertheless, we clearly see a shift of the minimum from oblate in ^{72}Rb to prolate in ^{76}Y. This assignment of ground-state deformations conforms with the previously suggested oblate and prolate shapes of the neighboring isobars, ^{72}Kr (see [31] and refs. therein) and ^{76}Sr (see [32] and refs. therein), respectively.

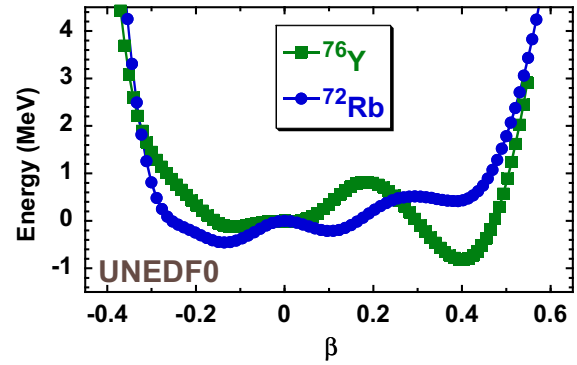

FIG. 8. Deformation energies as a function of the quadrupole deformation β calculated for ^{72}Rb and ^{76}Y using the Skyrme functional UNEDF0 [30].

At the predicted oblate ground-state deformation of ^{72}Rb, $\beta \approxeq -0.14$ (see Fig. 8), the most likely ground-state configuration is $\pi[321]3/2 \otimes \nu[321]1/2$. This gives the ground-state spin and parity of 1^+, which is in agreement with the known ground-state of the mirror nucleus ^{72}Br [33]. Here and below, we infer the total spins of configurations by assuming that blocked quasiparticle proton and neutron states are anti-aligned. This leads to the rule of $I = |K_\pi - K_\nu|$ that relates the total laboratory angular momentum I to projections K_π and K_ν of the intrinsic proton and neutron angular momenta, respectively, on the symmetry axis. Similarly, at the prolate ground-state deformation of ^{76}Y equal to $\beta \approxeq 0.40$, the proton (neutron) Fermi level is located next to the crossing between the [422]5/2 and [301]3/2 ([431]3/2 and [312]3/2) levels. Therefore, at deformations after or before the crossings one can have ground-state configurations of $\pi[422]5/2 \otimes \nu[312]3/2$ or $\pi[301]3/2 \otimes \nu[431]3/2$, respectively. However, only the configuration obtained after the crossing yields a spin-parity of 1^- that is consistent with the assigned ground-state spin-parity of the mirror nucleus ^{76}Rb [33]. Hence this configuration is tentatively assigned to the ground state in ^{76}Y.

We can see that the configurations and spin assignments of 1^+ and 1^- proposed in ^{72}Rb and ^{76}Y, respectively, conform to the Gallagher-Moszkowski (GM) rules [34]. However, as already noted in their paper, in $N \approxeq Z$ nuclei, these rules are not always obeyed. Indeed, by performing the angular-momentum projection of blocked quasiparticle states in the aligned or anti-aligned configurations, we could confirm that such configurations are always very close in energy, and hence that the GM rules for such nuclei are not very robust.

The above results suggest that the dominant configuration of the ground state in ^{72}Rb is most likely to be based on protons and neutrons occupying $l = 3$ orbitals and that the nucleus has a slightly oblate shape, ($\beta \approxeq -0.14$). On the other hand, the most favored ground-state configuration for ^{76}Y involves a proton in an $l = 4$ orbital and a neutron in an $l = 3$ orbit with the nucleus possessing a strong prolate deformation ($\beta \simeq 0.4$). These results provide a possible alternative explanation as to why ^{72}Rb undergoes proton decay (i.e., due to the lower deformation and lower angular momentum barrier) while ^{76}Y prefers to predominantly undergo β^+ decay.

V. SUMMARY

The ground-state lifetimes of ^{73}Sr and ^{76}Y have been determined for the first time and a more accurate value has been obtained for the lifetime of the ^{74}Sr ground state. In addition, further measurements have been made for the ground-state lifetimes of four other nuclei (^{70}Br, ^{71}Kr, ^{74}Rb, ^{75}Sr) which show very good agreement with previously published results. The results obtained for ^{73}Sr and ^{76}Y suggest that these isotopes are proton bound. These findings are compared with predictions of the proton driplines made by various calculations. The latter suggest that ^{73}Sr is one-proton bound, but that ^{76}Y is one-proton unbound, which is contrary to the experimental results. The experimental results indicate that the proton dripline resides in lighter mass nuclei than ^{73}Sr and ^{76}Y in the light strontium and yttrium region. Finally, a possible explanation, based on nuclear structure and deformation differences, for why ^{72}Rb undergoes proton decay while the α-conjugate nucleus ^{76}Y predominantly undergoes β^+ decay is presented in terms of new DFT calculations. These results are based on an assumption that it is the ground states that undergo proton (^{72}Rb) and β^+ (^{76}Y) decay. We note, however, that we cannot rule out the possibility that the observed decays in these nuclei may be due to excited states, with a 5^+ state in both nuclei being a possible candidate.

ACKNOWLEDGMENTS

We acknowledge the CSC-IT Center for Science Ltd., Finland, for the allocation of computational resources. We also thank James Cubiss for assistance with the final versions of the figures. This work was carried out at the RI Beam Factory (RIBF) operated by RIKEN Nishina Center, RIKEN and Center for Nuclear Study (CNS), University of Tokyo. The work was supported in part by the JSPS KAKENHI Grant No. 25247045 and UK Science and Technologies Facilities Council (STFC) Grants No. ST/M006433/1, No. ST/L005727/1, and No. ST/P003885/1. N.P.L. receives funding from the UK Department of Business Energy and Industrial Stratergy (BEIS) via the NMS programme.

[1] R. K. Wallace and S. E. Woosley, Astrophys. J. Suppl. **45**, 389 (1981).
[2] H. Schatz, A. Aprahamian, V. Barnard, L. Bildsten, A. Cumming, M. Ouellette, T. Rauscher, F.-K. Thielemann, and M. Wiescher, Phys. Rev. Lett. **86**, 3471 (2001).
[3] R. H. Burch, Jr., C. A. Gagliardi, and R. E. Tribble, Phys. Rev. C **38**, 1365 (1988).
[4] M. Oinonen *et al.*, Phys. Rev. C **56**, 745 (1997).
[5] G. C. Ball *et al.*, Phys. Rev. Lett. **86**, 1454 (2001).
[6] J. Huikari *et al.*, Eur. Phys. J. A **16**, 359 (2003).
[7] H. Suzuki *et al.*, Phys. Rev. Lett. **119**, 192503 (2017).
[8] T. Kubo *et al.*, Prog. Theor. Exp. Phys. **2012**, 03C003 (2012).
[9] P.-A. Söderström *et al.*, Nucl. Instr. Meth. B **317**, 649 (2013).
[10] N. Uematsu and S. Nishimura, RIKEN Accel. Prog. Rep. **41**, 151 (2008).
[11] S. Nishimura, Prog. Theor. Exp. Phys. **2012**, 03C006 (2012).
[12] S. Nishimura *et al.*, RIKEN Accel. Prog. Rep. **46**, 182 (2013).
[13] Z. Y. Xu *et al.*, Phys. Rev. Lett. **113**, 032505 (2014).
[14] J. Berkson, Ann. Stat. **8**, 457 (1980).
[15] K.-H. Schmidt *et al.*, Z. Phys. A **316**, 19 (1984).
[16] K. H. Schmidt, Eur. Phys. J. A **8**, 141 (2000).
[17] J. Henderson *et al.*, Phys. Rev. C **90**, 051303(R) (2014).
[18] H. Schatz, Int. J. Mass Spect. **251**, 293 (2006).
[19] I. Piqueras *et al.*, Eur. Phys. J. A **16**, 3 (2003).
[20] P. Kienle *et al.*, Prog. Part. Nucl. Phys. **46**, 73 (2001).
[21] J. C. Batchelder, D. M. Moltz, T. J. Ognibene, M. W. Rowe, R. J. Tighe, and J. Cerny, Phys. Rev. C **48**, 2593 (1993).

[22] P. Möller, A. J. Sierk, T. Ichikawa, and H. Sagawa, At. Data Nucl. Data Tables **109-110**, 1 (2016).
[23] B. A. Brown, R. R. C. Clement, H. Schatz, A. Volya, and W. A. Richter, Phys. Rev. C **65**, 045802 (2002).
[24] K. Kaneko, Y. Sun, T. Mizusaki, and S. Tazaki, Phys. Rev. Lett. **110**, 172505 (2013).
[25] G. A. Lalazissis, D. Vretenar, and P. Ring, Nucl. Phys. A **679**, 481 (2001).
[26] M. Wang, G. Audi, W. J. Huang, F. G. Kondev, S. Naimi, and X. Xu, Chin. Phys. C **41**, 030003 (2017).
[27] T. Faestermann *et al.*, Eur. Phys. J. A **15**, 185 (2002).
[28] Z. Janas *et al.*, Phys. Rev. Lett. **82**, 295 (1999).
[29] J. Uusitalo *et al.*, Phys. Rev. C **57**, 2259 (1998).
[30] M. Kortelainen, T. Lesinski, J. More, W. Nazarewicz, J. Sarich, N. Schunck, M. V. Stoitsov, and S. Wild, Phys. Rev. C **82**, 024313 (2010).
[31] J. A. Briz *et al.*, Phys. Rev. C **92**, 054326 (2015).
[32] E. Nacher *et al.*, Phys. Rev. Lett. **92**, 232501 (2004).
[33] Evaluated Nuclear Structure Data File (2019), http://www.nndc.bnl.gov/ensdf.
[34] C. J. Gallagher and S. A. Moszkowski, Phys. Rev. **111**, 1282 (1958).